Image and Vision Computing xxx (2009) xxx–xxx

Contents lists available at ScienceDirect

Image and Vision Computing

journal homepage: www.elsevier.com/locate/imavis

A highly accurate and computationally efficient approach for unconstrained iris segmentation

Yu Chen, Malek Adjouadi *, Changan Han, Jin Wang, Armando Barreto, Naphtali Rishe, Jean Andrian

College of Engineering and Computing, Florida International University, Miami, FL 33174, USA

ARTICLE INFO

Article history:
Received 15 December 2008
Received in revised form 7 April 2009
Accepted 27 April 2009

Keywords:
Biometric
Image processing
Color
Iris segmentation
Iris recognition
Hough transform
Step-length
Noise

ABSTRACT

Biometric research has experienced significant advances in recent years given the need for more stringent security requirements. More important is the need to overcome the rigid constraints necessitated by the practical implementation of sensible but effective security methods such as iris recognition. An inventive iris acquisition method with less constrained image taking conditions can impose minimal to no constraints on the iris verification and identification process as well as on the subject. Consequently, to provide acceptable accuracy measures, it is critical for such an iris recognition system to be complemented by a robust iris segmentation approach to overcome various noise effects introduced through image capture under different recording environments and scenarios. This research introduces a robust and fast segmentation approach towards less constrained iris recognition using noisy images contained in the UBIRIS.v2 database (the second version of the UBIRIS noisy iris database). The proposed algorithm consists of five steps, which include: (1) detecting the approximate localization of the eye area of the noisy image captured at the visible wavelength using the extracted sclera area, (2) defining the outer iris boundary which is the boundary between iris and sclera, (3) detecting the upper and lower eyelids, (4) conducting the verification and correction for outer iris boundary detection and (5) detecting the pupil area and eyelashes and providing means for verification of the reliability of the segmentation results. The results demonstrate that the accuracy is estimated as 98% when using 500 randomly selected images from the UBIRIS.v2 partial database, and estimated at ⩾97% in a "Noisy Iris Challenge Evaluation (NICE.I)" in an international competition that involved 97 participants worldwide, ranking this research group in sixth position. This accuracy is achieved with a processing speed nearing real time.

1. Introduction

Iris patterns are unique, and most evidently cannot be changed incidentally or intentionally, as the iris is a protected organ inside the human eye [1]. In view of this first affirmation, it is an accepted fact that among all potential biometric methods that make use of face, fingerprint and voice, among others, iris recognition remains the most viable and reliable biometric that is unrivaled when used for security reasons [2,3]. After J. Daugman proposed the first automatic iris recognition system [4] in 1993, a variety of commercial systems were developed to deal with eye images [5], which were taken under rigorous acquisition constraints. Under the current technological setups, and in order to take an adequate iris picture and take into consideration the different statistical properties [6], the subject must be still, look directly at the camera, and in a direction that satisfy strict illumination controls. This process is obviously time-consuming, and often inconveniences the subject [7]. With the increasing demands in public safety and security and with the necessity for critical/classified information access, secure identification is becoming a requisite that seeks high accuracy with a fast and reliable outcome. Thus, an effective iris recognition method is one that should initially overcome the rigid constraints imposed during iris image acquisition [8], and offer near real-time processing [9].

Nonetheless, serious noise effects are inherent in unconstrained iris recognition systems. Typical sources of noise include motion blur, defocus, eyelash or eyelid obstructions, specular reflection, among others. Traditional segmentation methods do not perform well under such conditions [10]. Thus, a good segmentation approach which can extract useful iris information from noisy iris images is a crucial first step. Consequently, the focus of this work is first placed on the development of a robust segmentation approach that can overcome such unpredictable noise effects in order to secure recognition outcomes with high accuracy. This first research step is complemented with efforts to optimize the processing speed, seeking near real-time. The UBIRIS.v2 [11] partial dataset, which contains 500 static eye images with more realistic noisy effects, as provided by the University of Beira Interior, was used to assess the merits of this method. Later, the executable

* Corresponding author. Tel.: +1 305 348 3019.
E-mail address: adjouadi@fiu.edu (M. Adjouadi).

0262-8856/$ - see front matter © 2009 Elsevier B.V. All rights reserved.
doi:10.1016/j.imavis.2009.04.017

program of the proposed method was also submitted for testing through an international contest "*Noisy Iris Challenge Evaluation (NICE.I)*" [12]. The approach we introduced here ranked us in the sixth position worldwide, considering that efforts were also devoted to making the processing speed of our approach as near real-time as possible. The next sections define the chronology of the aforementioned implementation steps.

2. Approximate localization of the eye area

There are five major stages contained in the proposed approach, as per the flowchart given in Fig. 1.

The images from the UBIRIS.v2 database were taken with the subject on the move and at different distances (between 3 and 7 m). Thus, the irises of the images may vary significantly in size and location. For the provided UBIRIS.v2 training dataset, the amount of pixels across the iris ranged from 75 to 190, and the iris may appear in any region within the close-up image. Therefore, as an initial step in the proposed approach, a method is used to approximately localize the eye part of the image, in order to obtain a smaller and more refined target area. This method, which is of considerable benefit in seeking accuracy and fast processing speed for segmentation purposes, consists of two steps: (1) finding an approximate eye area based on sclera detection, and (2) determining an adaptive target to confine the search for the iris.

2.1. Detecting the sclera area

Unlike conventional iris images, which are mostly captured under NIR (near-infrared) wavelengths with rigidly constrained environments, all the close-up images from the UBIRIS.v2 training dataset are full-color images taken under visible wavelength. For the UBIRIS.v2 dataset, the pupil area may not always appear darker than other parts, especially for images containing heavily pigmented (dark) irises or images with serious noise effects. Thus, the pupil on the image may no longer be the proper starting point to find the eye area. But through analyzing the full-color images, the sclera parts are commonly found to appear less saturated (white) than other parts of the images. Consequently, the sclera area is used instead for determining the target eye area.

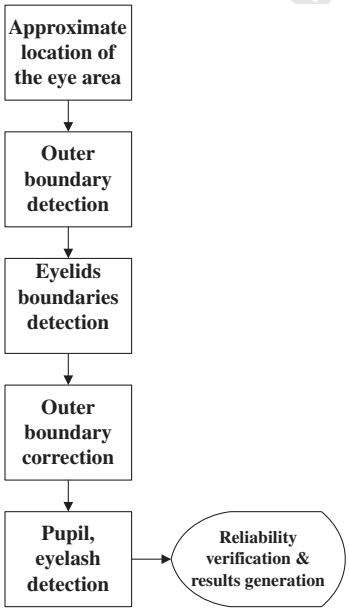

Fig. 1. The flowchart of the proposed approach.

The HSI color model decouples the intensity component from the color-carrying information (hue and saturation), and the saturation value of the HSI model refers to the degree of how much the white was added to the color [13]. Thus, the saturation value of the HSI model is more tolerant to noise effects for detecting the sclera area. Saturation value can be computed from the RGB values as given by Eq. (1).

$$S = 1 - \frac{3}{(R+G+B)}[\min(R,G,B)] \quad (1)$$

For the saturation value of the HSI model, when the pixel is white, $S = 0$; when the pixel is pure colored, $S = 1$. Through our experimental analysis, the saturation values of sclera areas provided a range from 0 to 0.21. The saturation value, which refers to sclera, would be calculated as a threshold, and all pixels below the threshold would be considered as pixels belonging to the sclera. That threshold is obtained by calculating the biggest group derivative within the range in a histogram of saturation values (between 0 and 0.21) corresponding to the image. With the threshold calculated from the original color image in Fig. 2(a) and (b) illustrates an example of extracting the sclera pixels from all other pixels, except for inherent noise points.

2.2. Determining a target area for the eye

The purpose of this step is to locate a target area with adaptive size in order to adjust for the different irises of the dataset. After the sclera detection step, it can be observed that some small spots of reflections and bright skin are scattered on the image as part of the sclera extraction step. Thus, more specific sclera areas need to be localized first, to overcome/eliminate the noise points. In opposition to the sclera part, all other spots extracted are generally smaller or slightly darker. The thresholded image, as in Fig. 3(b), is converted to a gray scale image, and for every pixel with a gray level intensity greater than 0, its value will be replaced by the average intensity value of a 17 * 17 block which is centered on that pixel. With this operation, the intensity of isolated and relatively smaller noise areas would be degraded significantly. For those pixels whose gray level intensities are greater than 0, the average intensity is calculated to be an adaptive threshold. With this threshold, a binary map which can clearly specify the sclera area can be generated.

The resulting binary maps, as can be seen, can be classified into two categories: double sclera, areas as shown in Fig. 3(a), and single sclera areas as shown in Fig. 3(c). In binary maps with double sclera appearing, the iris would certainly be located between them, and the rectangular area can be determined by the extreme coordinates of upper, lower, left and right locations of the two sclera areas, with a small offset proportional to the distance between these extreme points in relation to the image boundaries, in order to ensure inclusion of all the iris. The target rectangle given in Fig. 3(b) shows the result of a given image. With a single sclera

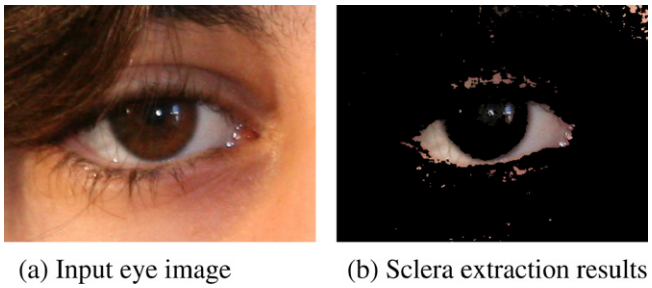

Fig. 2. Example of sclera detection in the presence of noise pixels.

Please cite this article in press as: Y. Chen et al., A highly accurate and computationally efficient approach for unconstrained iris segmentation, Image Vis. Comput. (2009), doi:10.1016/j.imavis.2009.04.017

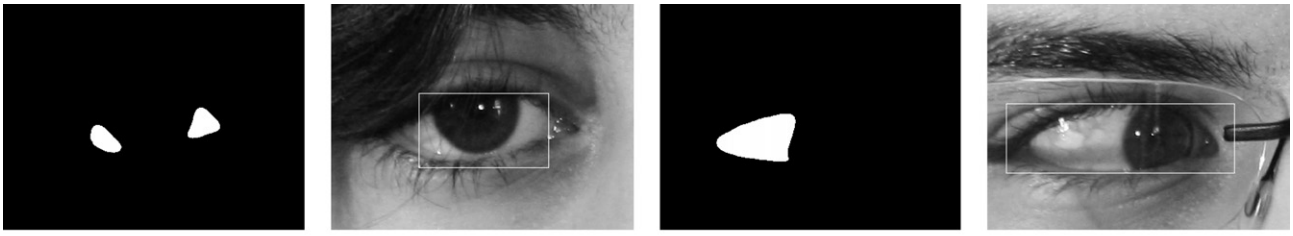

(a) Binary map of sclera (b) Target area delineation (c) Binary maps of sclera (d) Target area delineation

Fig. 3. Target selection for eye area based on double and single sclera areas.

area, as shown in Fig. 3(c), since it is unknown as to which side of the sclera the iris will be located, the nearest distances between the sclera area to the left and right boundaries of the image would be calculated, respectively. The rectangular area would be decided with respect to those distances. The longer the distance is, the more the rectangle would be extended towards the boundary in that direction. As shown in Fig. 3(d), the rectangle was mostly extended towards the right side, and as a result the iris part is within the rectangle, which correctly delineates the target area.

3. Iris outer boundary detection with a fast circular Hough transform

The outer boundary of the iris is defined as the boundary between iris and sclera. Because the Hough transform is based on a voting scheme, it is very tolerant to noise. To detect the outer boundary of noisy iris images from the UBIRIS.v2 database, the circular Hough transform was applied with some modifications to achieve higher accuracy and faster speed.

3.1. Detecting the outer boundary

To improve the performance of the circular Hough transform, some modifications were made towards both reducing the computational complexity as well as reducing the impact of inherent noise effects.

To generate the edge map, instead of the traditional four-direction Sobel edge detection [14], we only conducted the edge detection horizontally (left to right and right to left), as can be seen in Fig. 4(c); compared with Fig. 4(b), which was generated using four directions, the number of edge points was much reduced.

To improve the accuracy and processing speed, after generating the edge map similar to those in studies reported in [15–17], based on the information obtained from the previous step, the circular Hough transform would only be conducted using the edge points in the target rectangle. Also, some precautions are considered. First, the upper and lower limits of the radius can be set with respect to the size of rectangle. Thus, the upper limit of the radius is set as 1/2 of the rectangle's length, and the lower limit is set as 1/4 of the rectangle's width. Second, neither the center of the resulting circle center nor its boundary can possibly be located on the already defined sclera areas.

3.2. A fast circular Hough transform

Although the circular Hough transform is a powerful algorithm, it also carries with it a heavy computational accumulator, and that refers to the three step iterations burden. With the circular Hough transform, each edge point (x, y) in the image space votes for (a, b, r) in the parameter space for each possible circle passing it, where a, b are the coordinates of the circle center position, and r being the radius of the circle. Thus, the votes were cast in a three-directions accumulator for conducting the circular Hough transform. If O_1 is the computational complexity of calculating votes for a circle with a determined center location and radius, the computational complexity of the circular Hough transform O_a would be as given by Eq. (2):

$$O_a = (a_{\max} - a_{\min}) * (b_{\max} - b_{\min}) * (r_{\max} - r_{\min}) * O_1 \quad (2)$$

Here the step-length was applied to reduce the computational burden of the circular Hough transform. Let C_a, C_b, C_r be the step-length for the parameters a, b, c, respectively, then the computational complexity would be as given by Eq. (3):

$$O_b = (a_{\max} - a_{\min}) * (b_{\max} - b_{\min}) * (r_{\max} - r_{\min}) * O_1/(C_a * C_b * C_r) \quad (3)$$

In the implementation of the proposed approach, the step-lengths are set such that $C_a = C_b = C_r$.

Because of the three step-lengths, a large number of votes will not be counted. To overcome this problem, with a determined circle center and radius, instead of only searching for the edge points located on the circle, all points located on the circular ring surrounding that circle would be counted. For instance, as shown in Fig. 5, instead of searching for edge points located on the solid circle 1, the search will also include all points within the dashed circles A and B; similarly, all points within dashed circle B and C would count as votes for the target searching circle given by solid circle 2.

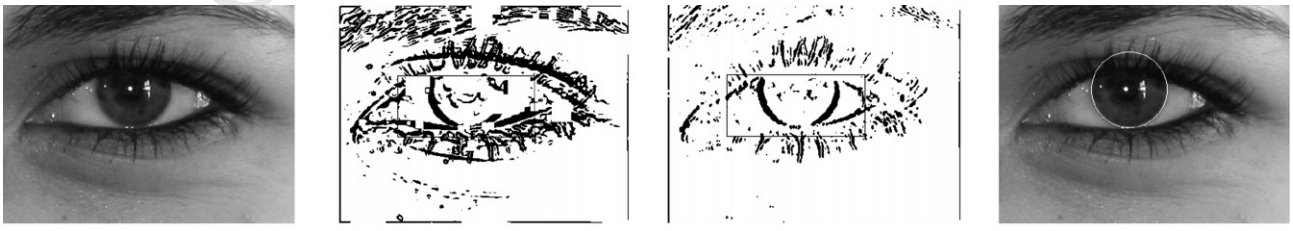

(a) Input image (b) Edge map of 4 directions (c) Edge map of 2 directions (d) Boundary detection result

Fig. 4. Example of outer boundary detection using the modified circular Hough transform.

Please cite this article in press as: Y. Chen et al., A highly accurate and computationally efficient approach for unconstrained iris segmentation, Image Vis. Comput. (2009), doi:10.1016/j.imavis.2009.04.017

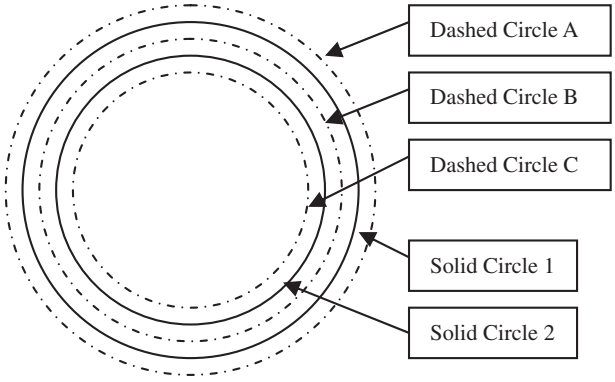

Fig. 5. Example of searching feature points locating on the circular ring around the target circle.

We also accelerate the step of searching for all the edge points located on the circular rings. We implement the algorithm with dynamic programming method [18]. Initially, the distance between every pixel point on the image and the image center point would be calculated, all those distances would be stored in the table, and each distance would refer to a list of relative locations which have that certain distance from the center location of the image frame. When searching for the edge points on the circle, the neighboring distances would refer to a set of relative locations in the look-up table, and all edge points located on the corresponding locations in the image would be counted. Because the look-up table was generated just after executing the proposed approach for a single image, and since the size of all input images is 400 * 300, there is no need to calculate distances while performing the Hough transform for each image, and the computational burden was consequently alleviated significantly.

Finally, to obtain more consistent results, instead of just choosing the peak value of votes in the parameter space, a range of highest values (for this research, all the parameters have a value within 5% of the peak value votes) are used instead; by examining their neighboring parameters which are bypassed because of using step-length, more precise results can be accomplished.

To demonstrate the performance of the proposed method, the step-length is set to be between 1 and 5, and the processing time is examined based on all 500 eye images from the UBIRIS.v2 training database. The results are as shown in Fig. 6, where the step-lengths for C1 through C5 are 1 through 5, respectively.

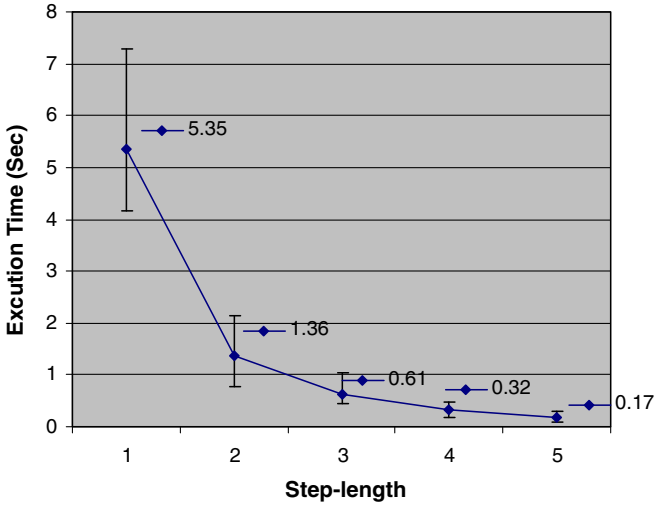

Fig. 6. Average processing time for circular Hough transform using 500 images from the UBIRIS.v2 training database.

This modified circular Hough transform decreases the execution time of the proposed approach significantly. The average processing time using the circular Hough transform which applies a step-length of 1 is calculated as 6.77 s per image, and the error rate of such an approach is estimated at 0.0200215 in the E1 measure provided by the Committee of NICE.I. With the proposed modified circular Hough transform, the average execution time is decreased to 0.83 s and the E1 error rate is 0.0200823 now. With the proposed modified Hough transform, the execution time is significantly decreased by 8.2 times, while the accuracy is only degraded by 0.303%, which is considered negligible. Execution time and E1 error rates for both cases are examined by processing the provided 500 iris images from the UBIRIS.v2 database using a laptop computer with 1.86 GHz CPU (Intel T1350 solo) and 2 GB of RAM. The executable program we submitted to the NICE.I committee is the fast version, which used the modified circular Hough transform with a step-length of 5.

4. Boundary detection of the upper and lower eyelids

In unconstrained iris acquisition scenarios, as the subject is not required to comply with a demanding level of cooperation, it is observed that considerable eyelid occultations often occur. The linear Hough can be applied to the edge map of the eye image to detect the eyelids. However, with this algorithm, the key problem for dealing with noisy eye images is that the obtained edge maps are usually non-ideal. As shown in Fig. 7(a), most edge points appearing on the map are undesired, caused by eyelids, reflections inside the iris, and the texture of the iris patterns. To overcome this problem, an improved strategy for eyelid detection is proposed. Because the slopes of the upper and lower eyelids are not steep in most cases, the proposed approach starts by applying edge detection in only the vertical direction. The generated edge map will have an emphasis on the desired eyelids edge points. Fig. 7(a) is one such example.

The proposed approach has shown good performance for processing noisy iris images from the UBIRIS.v2 dataset. Fig. 7 illustrates an example for eyelid boundary detection.

To distinguish the points which are edges between iris and eyelids, a patch of area is selected to calculate the average gray intensity I_A of the iris, as shown in Fig. 8. A square patch just below the pupil is chosen, since this area is experimentally determined to be the one most unlikely to be affected by reflections or overlap with eyelids. Because iris sizes vary significantly within the given UBIRIS.v2 dataset, the size of the patch is set to be adaptive in relation to the size of the iris. For this research we set the length of the square to be $R_{outer}/10$, with R_{outer} being the radius of outer iris boundary. The upper boundary of the patch is $R_{outer}/8$ below the pupil's lower boundary.

With the outer boundary circle obtained as in Fig. 7(d), rays are traced starting from the center of the circle and toward every point on the upper or lower arc of the circle (central angle $\theta = 120°$). For each ray, if an edge point was found, M points beyond this point in the ray's direction would be verified using the average gray scale I_A to see if it is within a range of $I_A \pm 10\%$; if N of M points can be considered as points on the iris, the found edge point would be ignored in order to eliminate potential smaller reflection regions and iris regions with textural properties, and the search would go on until reaching the circle boundary. For this implementation, $M = R_{outer}/6$ and $N = R_{outer}/10$. The example shown in Fig. 7(d) shows the verified edge points for the upper eyelid. After the verified edge map was generated, the linear Hough transform was then used. Since most of the undesired edge points were removed before this step,

Please cite this article in press as: Y. Chen et al., A highly accurate and computationally efficient approach for unconstrained iris segmentation, Image Vis. Comput. (2009), doi:10.1016/j.imavis.2009.04.017

(a) Sobel edge detection (b) Upper eyelid boundary (c) Left eyelid boundary (d) Eyelid boundary detection

Fig. 7. Example for detecting upper and lower eyelids within the given the UBIRIS.v2 dataset.

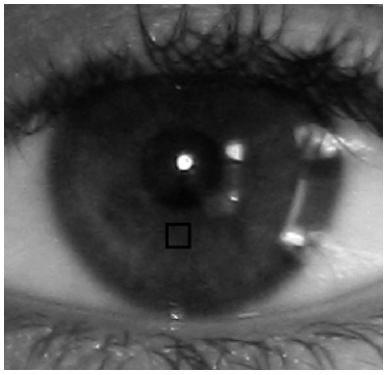

Fig. 8. Example of the square patch used to obtain the average gray intensity.

the results of the linear Hough transform would be more accurate and more tolerant to noise.

For some cases, it would be more accurate to describe the eyelid with multiple lines. In the proposed approach, after the first line was detected, the edge points on that line were moved and so were all edge points located within 5 pixels above and below that same line. The linear Hough transform is then applied again, and if there are enough votes, another line would be determined, and so on. Then point removal and Hough transform would be applied again. This process would continue until the peak value of the linear Hough transform is below a threshold, which for this research is set as $R_{outer}/4$. Fig. 7 shows an example of these cases. Fig. 7(b) shows the detected points which are on the edge of iris and upper eyelid, Fig. 7(c) shows the remaining points after the first linear Hough transform for the upper eyelid, Fig. 7(d) shows the final results of boundary detection for upper and lower eyelids. Two other results from the UBIRIS.v2 database are shown in Fig. 9 for comparative purposes.

5. Circle correction and non-circular boundary detection

Although the outer iris boundary was assumed to be circular for most of the conventional iris segmentation methods, it has been pointed out that human iris boundaries are usually non-circular [19] The error caused by defining the boundary as a circle is especially crucial for less constrained iris recognition, because of ubiquitous off-angle effects during non-cooperative iris acquisition. Also the circular Hough transform can generate inaccurate results due to noise. For this reason, a strategy was developed to define the non-circle boundary and correct the inaccurate result obtained from the circular Hough transform.

Fig. 9. Results of the detection of the eyelid boundaries.

Fig. ~~10 (a)~~ is one example of outer boundary detection error caused by a non-circular iris boundary. As can be seen, the outer boundary cannot be correctly detected. The proposed verification and correction method is based on three steps; the first step is the circle center verification, the second step is multiple circle (or arc) searching, the third step is multiple arcs and lines connection.

There is a need to find the correct center of the iris to verify the original circle center found from the first Hough circle transform. Shown in Fig. 10(b) is a square grid with an adaptive size inside the outer iris boundary. The center of the grid which yields the lowest average gray intensity would be selected as the correct outer iris boundary center. For the purpose of this research, if the Euclidean difference between the original center and the newly detected one is greater than $R_{outer}/4$, the original outer boundary would be assumed as inaccurate. Then a target area would be selected for conducting Hough circular transform again. Based on the experimental study, the desired iris boundary is usually inside the Hough circle. The reason for this is that the edge points outside the iris usually vote for larger circles and for an off-angle iris which is usually smaller than its actual size. Thus, the target area whose center is at (x_t, y_t) as shown in Fig. 11 was expected to be the region between the real iris center (x_r, y_r) and the arc on the opposite side of the original circle.

In reference to Fig. 11, the center of the target rectangle is (x_t, y_t), and the original circle center is (x_c, y_c), here we have:

$$y_t = y_c, \quad \text{and} \quad x_t = x_c - (x_r - x_c) \quad \text{or} \quad x_t = 2x_c - x_r \tag{4}$$

Another Hough transform will be conducted to the edge points inside the target rectangle. Because the goal is to detect a circle which is usually partially located on the target region, different weights are set to the votes generated inside and outside of the target region to get more accurate results. In our experiments, we set the weight of the vote as 1 for the outside region and as 7 for the inside region.

Since the Hough transform is based on voting, to avoid uncertain results, an adaptive voting count threshold is set such that if the highest voting count is below this threshold, the circle will not be generated. This threshold is set as $T = M * 35\%$, where M is the total count of edge points in the target rectangle. If the peak value $N < M$, the circle will not be considered. The black circle shown earlier in Fig. 10(e) is one outcome example of this step.

The intersection of two circles can be used to describe the non-circular iris. The upper and lower eyelids lines are also used here to remove unexpected eyelids and eyelashes. Thus, as can be seen

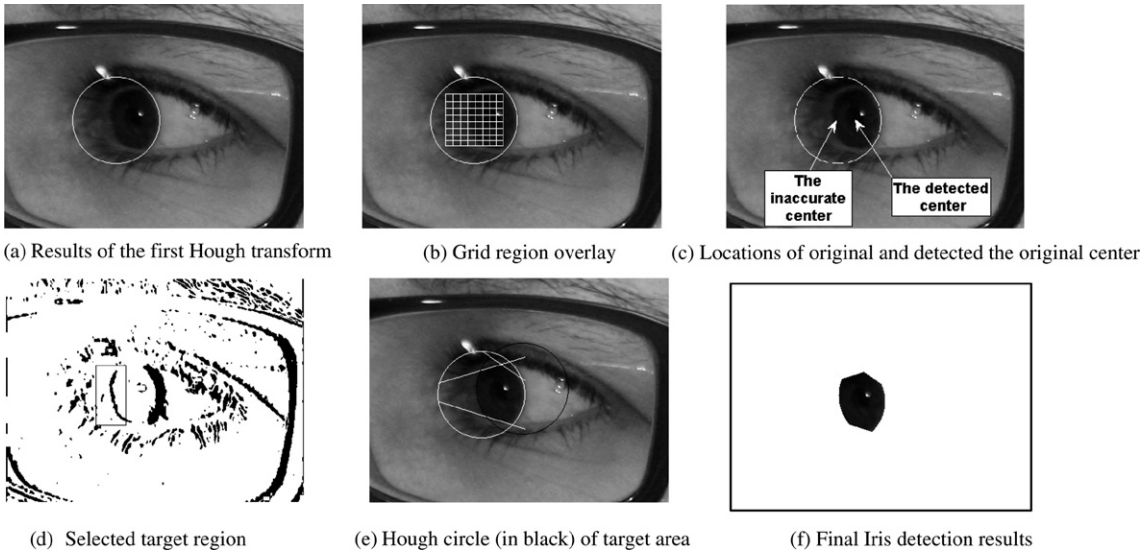

(a) Results of the first Hough transform (b) Grid region overlay (c) Locations of original and detected the original center

(d) Selected target region (e) Hough circle (in black) of target area (f) Final Iris detection results

Fig. 10. Defining the non-circular iris boundary – the intersection of the two circles with the detected eyelids lines is the accrual iris.

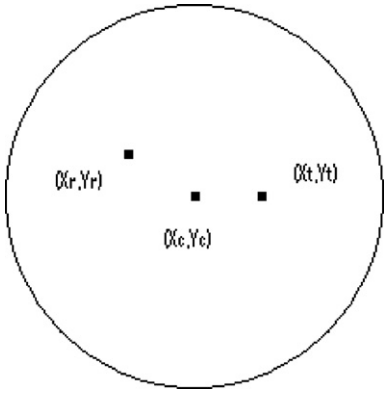

Fig. 11. Relations between the real iris center, original circle center and center for target rectangle.

from Fig. 10(f), the final result of the detected boundary consists of multiple arcs and lines, and would be more accurate for describing non-circular iris boundaries. Other examples provided for comparative purposes are shown in Fig. 12.

Inaccuracies introduced by the circular Hough transform can thus be resolved with the proposed method. As shown in Fig. 12, the larger circles shown in (a) and (b) are inaccurate circular Hough transform results, and the smaller circles in both cases are the newly detected ones through the proposed method. As can be seen, the intersections are much more accurate. Fig. 12(c) and (d) are two other examples with different iris sizes and different eye gazes. The left circle shown in Fig. 12(c) and the right circle shown in Fig. 12(d) are the original Hough transform results, which, as can be seen, are slightly off from the expected result.

6. Pupil, eyelash detection and results reliability verification

Because the eye images from the UBIRIS.v2 dataset were captured under visible wavelength, one of the major differences with those images taken under NIR wavelength is that the intensity contrast of iris and pupil can be very low, especially for heavily pigmented (dark) irises, such as in Fig. 13(a). Thus, pupil removal is left for this step to be performed; with only iris and pupil, the contrast enhancement method would yield better performance.

As shown in Fig. 13, image (a) is the outcome from the previous step (outer iris and upper and lower eyelid boundary delineation). We used an empirical intensity threshold of 150 to detect the reflections, and expanded every reflection point by a 3 * 3 mask to ensure its total removal. Then, histogram equalization was applied to get the high-contrast image, as shown in image (b). Sobel edge detection was used to get the edge map (c), and then the circular Hough transform determined the pupil boundary. Caution is taken such that the pupil center should be located within the small white circle shown in Fig. 13(b) with a radius of $R_{outer}/10$, and its center can be considered as the outer iris center. The radius of the pupil boundary is set to be from $3R_{outer}/20$ as a lower limit to $11R_{outer}/20$ as the upper limit. Fig. 13(d) shows the result for this illustrative example. To detect the eyelashes, we set an adaptive empirical threshold to be $0.45 * I_A$, where I_A is the obtained average iris color as described in Section 4. The eyelash removal would be

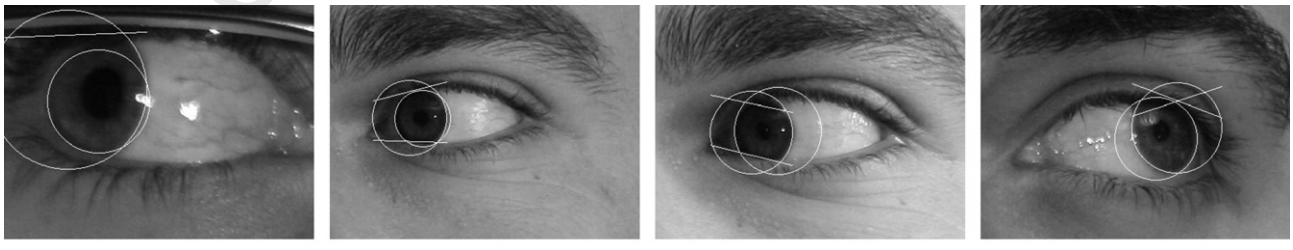

(a) Circle correction: case 1 (b) Circle correction: case 2 (c) Delineating iris boundary (d) Delineating iris boundary

Fig. 12. Result examples of proposed circle verification and correction strategy for delineating non-circular iris boundaries.

Please cite this article in press as: Y. Chen et al., A highly accurate and computationally efficient approach for unconstrained iris segmentation, Image Vis. Comput. (2009), doi:10.1016/j.imavis.2009.04.017

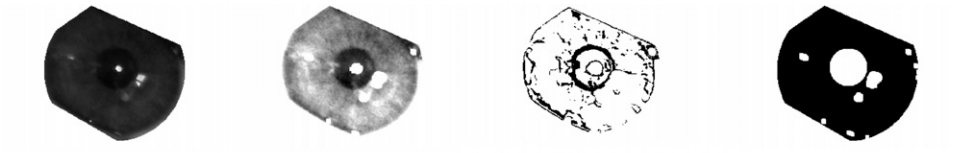

(a) Iris image with pupil (b) Contrast enhancement (c) Result of edge detection (d) Pupil removal result

Fig. 13. Process for pupil detection and removal.

performed within the top $R_{outer}/3$ part of iris. After the pupil and eyelash removal, the result of the segmentation approach would be generated.

To ensure that the falsely segmented results would not pass to the next step of iris recognition, a reliability verification procedure was applied to minimize false positives. For the UBIRIS.v2 dataset, if the segmented iris is too big ($R_{outer} > 120$), too small ($R_{outer} < 20$), too bright ($I_A > 90$), or if the average intensity of the pupil is brighter than the average iris intensity, the segmented result would be rejected.

7. Result and discussion

Some of the good results are shown in Fig. 14. The green and red parts on the iris area are the non-matched errors as determined by the NICE.I committee through an unbiased evaluation.

As shown in Fig. 14, almost all the function modules of the proposed approach worked very well. Some errors occurred on the outer iris boundary, because a single circle is used to define the boundary, but those errors are relatively small.

Through the same unbiased evaluation, some of the worst results were caused by sclera detection errors, as shown in Fig. 15(a). For this image, the sclera area was found to be the bright part of the upper eyelid; thus, the target rectangle was falsely set to be out of the iris region. Fig. 15(b) shows that with an incorrect searching target area, unpredictable results would be obtained from the circular Hough transform; the black circle on the top-right of the image is the outcome of iris boundary detection which was conducted in the non-iris region. In the results given in Fig. 15(c), the green area refers to false positive errors, and the red area refers to false negative errors.

As for the example given in Fig. 15(d), because the white wall behind the subject is detected to be sclera, the target rectangle was set to be too large for the actual iris region, and the upper limit radius of the target circle was set to be too large (recall that the upper limit of the radius is set to be half of the rectangle length in the proposed approach). As shown in Fig. 15(e), in that search area, a very large circle can get more votes than the actual boundary circle. Thus, as shown in Fig. 15(f), incorrect results are obtained, with the red (false negative) being small because the incorrect result region incidentally covers the real iris area.

The UBIRIS.v2 dataset includes rotated iris images, and some of which with the angles that are more than 30° (relative to the horizontal). Through our experiments on the provided training dataset, it has been noticed that the rotation effects may impact the step of locating the target iris area which is introduced in Section 2.2, although those impacts are mostly overcome. There are 17 images with the rotations greater than 30° relative to horizontal, and only two cases lead to inaccurate iris outer boundary detection results.

As the target rectangle area is set to be a horizontal rectangle, for those rotated iris images, the determined target rectangle may cover a partial iris area instead of the whole iris area. Because the voting based circular Hough transform would be used to search for the outer iris boundary, a partial circle within the target area can still determine the outer boundary. Furthermore, the target rectangle area is extended with respect to the location and size of the sclera area; and for most of the rotated iris images, an adequate portion of the iris would still be covered, providing desirable outer boundary detection results even under these extreme conditions.

As shown in Fig. 16(b), although the target rectangle does not cover the whole iris boundary, the rectangle is extended downwards to cover more of the boundary edge points. The white circle drawn in Fig. 16(c) shows the accurate result of outer boundary detection. An inaccurate outer boundary detection caused by rotation effect is also given in Fig. 16(d)–(f). As can be seen in Fig. 16(e),

Fig. 14. Examples yielding good results.

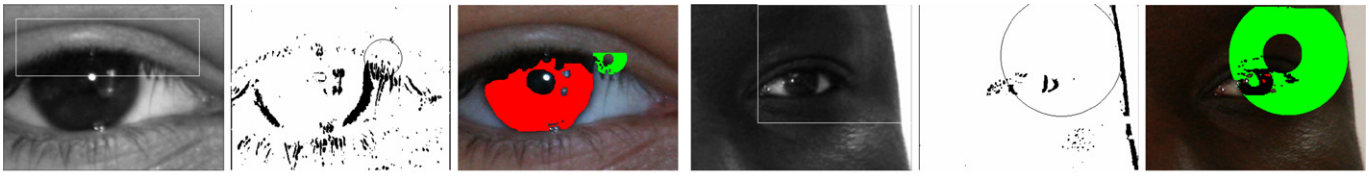

(a) Eye area selection (b) Iris boundary detection (c) Error (d) Eye area selection (e) Iris boundary detection (f) Error

Fig. 15. Examples yielding faulty or undesired results.

Please cite this article in press as: Y. Chen et al., A highly accurate and computationally efficient approach for unconstrained iris segmentation, Image Vis. Comput. (2009), doi:10.1016/j.imavis.2009.04.017

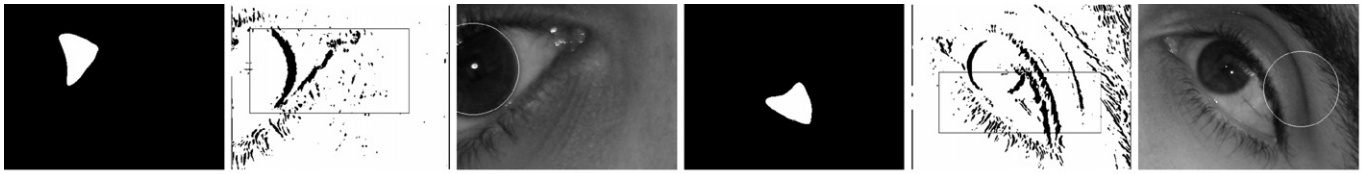

(a) Binary map (b) Target area on edge map (c) Accurate result (d) Binary map (e) Target area on edge map (f) Inaccurate result

Fig. 16. Examples of detecting the outer iris boundary of rotated iris images.

since the detected sclera area is located just below the middle of the image, the target is slightly_extended upwards. The target rectangle covers relatively a small portion of the iris area; with other noise effects on the edge map such as eyelashes and eyelids. The inaccurate outer boundary detection resulted as reflected by the white circle drawn in Fig. 16(f), due to inaccurate positioning of the rectangle.

In retrospect, through the unbiased evaluation from NICE.I committee, the results of the proposed approach yielded error measures of E1 = 0.029 and E2 = 0.163 (where False Positive rate = 0.018 and False Negative rate = 0.307). E1 and E2 are defined in detail in the NICE.I Evaluation webpage (http://nice1.di.ubi.pt/evaluation.htm). The results obtained with the proposed approach ranked us sixth of all 97 participants worldwide.

Just as important, the processing speed of our approach is fast. For the 500 images from provided UBIRIS.v2 training dataset, the average processing time for each iris image is 0.83 s per image. The result is gotten from a laptop computer with 1.86 GHz CPU (Intel T1350 solo) and 2 GB of RAM. The proposed approach was implemented using C++ programming language.

8. Conclusion

This study proposed a new and robust approach for iris segmentation on less constrained iris acquisition scenarios. It produced high performance in eye images from the UBIRIS.v2 database, which contains very realistic noise effects. The accuracy of the proposed approach was evaluated as part of the NICE.I contest, ranking the method with the sixth lowest error rate among 97 participants worldwide. This accuracy is augmented in merit by the fact that the processing speed of the proposed approach is near real-time, requiring only 0.83 s to perform all the required steps for a final iris segmentation.

The proposed approach relies on an effective search for the sclera area of the image. A threshold of saturation value (the HSI model) was obtained by calculating the biggest group derivative of the histogram of the original color image. Then, to remove the remaining undesired reflections or bright skin, the value of every non-black pixel was replaced by the average intensity value of a 17 * 17 block around it. A binary map was thus generated to indicate the sclera area. This process allowed for a narrower target area with respect to the size and the location on the image of the sclera in order to accelerate the circle search process for the outer iris boundary detection.

The outer boundary of the iris was detected using a modified fast Hough circular transform. The modifications considered were specifically established to alleviate the computational burden of the original Hough transform while still seeking a highly accurate segmentation outcome. In this approach, the same step-length is used for the three step iterations of the Hough circular transform, yielding a significantly faster processing speed. The use of this step-length is complemented with an optimization method designed to yield more accurate results.

The third step focused on detecting the upper and lower eyelids. To overcome various noise effects, a new approach was devised to identify the edge points located on the boundary between eyelid and iris. The identification is based on verifying whether each edge point actually belong to the eyelid and not to the iris region. A linear Hough transform is used recursively to extract the edges of eyelids.

A new method for verification and correction for the outer iris boundary was also proposed. The new strategy consisted of (1) verifying and correcting the center position of the outer iris boundary, (2) localizing the target region, (3) performing Hough circular transform with different weights in and out of the target region and (4) verifying the reliability of the results in terms of the number of edge points which actually belong to the boundary of the iris. As a result, multiple arcs and lines were used to delineate a non-circular iris boundary, and correct the initial inaccurate results of the circular Hough transform.

For the final step, in order to generate a more accurate pupil boundary in the edge map, histogram equalization was used to enhance the contrast between the iris and pupil. Consequently, the extracted pupil area is removed from further consideration, allowing for an iris recognition process to focus solely on the delineated iris area.

References

[1] R.P. Wildes, Iris recognition: an emerging biometric technology, Proc. IEEE 85 (9) (1997) 1348–1363.
[2] L. Ma, T. Tan, Y. Wang, D. Zhang, Personal identification based on iris texture analysis, IEEE Trans. Pattern Anal. Mach. Intell. 25 (12) (2003) 1519–1533.
[3] J. Daugman, How iris recognition works, IEEE Trans. Circ. Syst. Video Technol. 14 (1) (2004) 21–30.
[4] J. Daugman, High confidence visual recognition of persons by a test of statistical independence, Trans. Pattern Anal. Mach. Intell. 15 (11) (1993) 1148–1161.
[5] E. Newton, P.J. Phillips, Meta-analysis of third party evaluations of iris recognition, Biometrics Theory Appl. Syst. (September) (2007) 1–4.
[6] J. Daugman, The importance of being random: statistical principles of iris recognition, Pattern Recognit. 36 (2) (2003) 279–291.
[7] H. Proença, L.A. Alexandre, Toward noncooperative iris recognition:a classification approach using multiple signatures, IEEE Trans. Pattern Anal. Mach. Intell. 29 (4) (2007) 607–612.
[8] J.R. Matey, O. Naroditsky, K. Hanna, R. Kolczynski, D. Lolacono, S. Mangru, M. Tinker, T. Zappia, W.Y. Zhao, Iris on the move: acquisition of images for iris recognition in less constrained environments, Proc. IEEE 94 (11) (2006) 1936–1946.
[9] Y. Chen, J. Wang, M. Adjouadi, A robust segmentation approach to iris recognition based on video, in: Applied Imagery Pattern Recognition (AIPR) Annual Workshops, Washington, DC, October 15–17, 2008, IEEE, 8 p., ISBN: 978-1-4244-3125-0.
[10] W. Kong, D. Zhang, Detecting eyelash and reflection for accurate iris segmentation, Int. J. Pattern Recognit. Artif. Intell. 17 (6) (2003) 1025–1034.
[11] H. Proença, L.A. Alexandre, UBIRIS: a noisy iris image database, in: Springer Lecture Notes in Computer Science – ICIAP 2005: 13th International Conference on Image Analysis and Processing, vol. 1, Cagliari, Italy, September 6–8, 2005, pp. 970–977, ISBN: 3-540-28869-4.
[12] H. Proença, L.A. Alexandre, The NICE.I: Noisy Iris Challenge Evaluation – part I, in: Proceedings of the IEEE First International Conference on Biometrics: Theory, Applications and Systems – BTAS 2007, Washington, DC, USA, September 27–29, 2007, ISBN: 978-1-4244-1597-7.

Please cite this article in press as: Y. Chen et al., A highly accurate and computationally efficient approach for unconstrained iris segmentation, Image Vis. Comput. (2009), doi:10.1016/j.imavis.2009.04.017

[13] R. Woods, R. Gonzales, Digital Image Processing, second ed., Prentice-Hall, Upper Saddle River, NJ, 2002. pp. 295–301.
[14] J. Kittler, On the accuracy of the Sobel edge detector, Image Vis. Comput. 1 (1) (1983) 37–42.
[15] F. Candocia, M. Adjouadi, A similarity measure for stereo feature matching, IEEE Trans. Image Process. 6 (10) (1997) 1460–1464.
[16] M. Adjouadi, F. Candocia, X. Zhang, John Riley, Exploiting Walsh-based attributes in stereo vision, IEEE Trans. Signal Process. 44 (2) (1996) 409–420.
[17] M. Adjouadi, F. Candocia, A stereo matching paradigm based on the Walsh transformation, IEEE Trans. Pattern Anal. Mach. Intell. 16 (12) (1994) 1212–1218.
[18] R. Bellman, Dynamic Programming, Princeton University Press, Dover, 2003. pp. 81–115, ISBN: 0486428095.
[19] X. Liu, K.W. Bowyer, P.J. Flynn, Experimental evaluation of iris recognition, in: Proceedings of Face Recognition Grand Challenge Workshop, FRGC 05, vol. III, 2005, p. 158.

Please cite this article in press as: Y. Chen et al., A highly accurate and computationally efficient approach for unconstrained iris segmentation, Image Vis. Comput. (2009), doi:10.1016/j.imavis.2009.04.017